Heliyon 10 (2024) e32240

Contents lists available at ScienceDirect

Heliyon

journal homepage: www.cell.com/heliyon

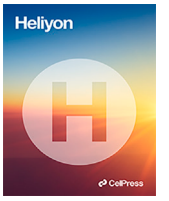

Research article

# Prediction of constitutive model for basalt fiber reinforced concrete based on PSO-KNN

Meng Zhu [a], Jiajian Lin [a,*], Guangyong Cao [b,c], Junliang Zhang [a], Xin Zhang [a], Jiaxing Zhou [a], Yang Gao [a]

[a] School of Electrical Engineering and Automation, Anhui University, Hefei 230601, PR China
[b] School of Civil Engineering, Anhui Jianzhu University, HeFei 230601, PR China
[c] Anhui Provincial Key Laboratory of Building Structure and Underground Engineering, Hefei 230601, PR China

ARTICLE INFO

*Keywords:*
Basalt fiber concrete
Particle swarm
K-nearest neighbor
Constitutive model

ABSTRACT

In order to find a simple method to study the effect of basalt fibers on the mechanical properties of concrete when incorporated into concrete, machine learning is introduced in this work on an experimental basis. The basalt fiber-reinforced concrete (BFRC) specimens were fabricated through independent processing, and the compression tests under different stress states were conducted on the BFRC specimens with different fiber compositions using the MTS816 rock testing system. After obtaining the experimental dataset with the four influencing factors of fiber volume fraction, fiber length, circumferential pressure and strain as input variables and stress as output variable, the BFRC prediction model was established based on extreme gradient boosting, support vector machine, K-nearest neighbor, and Particle Swarm Optimization K-Nearest Neighbor (PSO-KNN) algorithms; Then the predicted fitting results of the training set and test set are analyzed according to the relevant evaluation indexes, and the data indexes indicate that the PSO-KNN model has the best prediction performance, and the PSO-KNN model is used to predict the stress-strain fitting curves of BFRC, and finally the parameter contribution is analyzed based on the information of the curves. This is the first time that PSO-KNN is used in the study of BFRC eigenmodel, and the prediction effect is good, which not only overcomes the drawbacks of time-consuming and expensive experimental research, but also provides a basis and reference for engineering applications and later scholars' research on BFRC eigenmodel.

## 1. Introduction

Basalt fiber (BF) is a new type of inorganic, environmentally friendly, green, and high-performance fiber material. BF has excellent temperature resistance, monofilament mechanical strength, elastic modulus, density, creep fracture stress, chemical stability and other physical and chemical properties [1]. Its corrosion resistance is better than ordinary glass fiber, and its mechanical performance index is also about 30% better than ordinary glass fiber. The creep rate is about 1/4 of aramid fiber, and the process energy consumption is about 1/16 of carbon fiber. Its application fields include national defense and military industry, civil engineering facilities, building reinforcement, ocean engineering, ultra-high voltage power transmission, rail transit vehicles, automotive lightweight, fire protection, environmental protection, etc. [2][3]. BF is an inorganic silicate fiber with natural compatibility with

* Corresponding author at: School of Electrical Engineering and Automation, Anhui University, Anhui, HeFei, China.
*E-mail address:* jjlin@ahu.edu.cn (J. Lin).

https://doi.org/10.1016/j.heliyon.2024.e32240
Received 30 March 2024; Received in revised form 30 May 2024; Accepted 30 May 2024

Available online 4 June 2024

silicate materials (cement, concrete), and has technical advantages in the fields of asphalt sealing, cement reinforcement, and concrete reinforcement [4]. Taking the reinforced concrete structure as an example, the shortcut BF mixed with the cement matrix can form a uniform three-dimensional traction "micro skeleton" system, which can withstand the shrinkage deformation stress, increase the material toughness, improve the component ductility, inhibit cracks [5][6], and is a cost-effective reinforcement material. Compared to ordinary concrete, basalt fiber reinforced concrete (BFRC) exhibits the following three specific aspects in terms of quality performance:

① The compressive strength of BFRC has been increased by about 2.6%, and its frost resistance has also been improved to some extent.

② BFRC splitting tensile strength increased by 9.8%, Flexural strength increased by 15.3%, and bending ultimate tensile length increased by 19.1%, which helps to delay the formation of initial cracks and reduce microcracks caused by concrete shrinkage.

③ BF reinforcement materials can effectively replace steel, alleviate engineering problems such as metal material corrosion and maintenance, and improve the durability and safety of concrete structures [7][8].

At present, many research results have confirmed that adding BF to concrete can improve various mechanical properties of concrete [9][10]. For example, Wei Chen et al. [11] simulated the cubic compression, axial compression, and splitting tensile behavior of BFRC specimens by controlling the BF content. By comparing the test data with the simulation results, it was confirmed that the compressive strength of concrete will be correspondingly enhanced when BF is added. Zhao Yanru et al. [12] also studied the stress-strain relationship in the stress-rising stage of BFRC. However, at present, there are few studies on the whole process Stress-strain curve of BFRC under uniaxial compression, but it is an essential constitutive model for ultimate bearing capacity analysis and nonlinear whole process analysis of concrete members [13]. The study of stress-strain behavior of concrete is a very important aspect of its mechanical properties, and is crucial for the design and use of safe concrete in engineering. Therefore, the necessity of conducting experimental research on the constitutive model of BFRC is obvious [14–16]. However, the experimental process of studying the stress-strain behavior of BFRC through experimental methods is lengthy, cumbersome and labor-intensive, and the instruments, equipment, and specimen materials are expensive. To break through the limitations of the experimental path, scholars have continuously applied machine learning methods to predict various mechanical properties of concrete [17–19]. For example, Yakowitz [20] first applied the k-nearest neighbors (KNN) method to prediction tasks in 1988. Clark [21], Turochy [22], and Kindzerskel [23] further studied the algorithm from the coefficient selection of distance parameter p, K-value search, and distance weight. Li Hong et al. [24] used genetic algorithm to optimize the kernel Extreme learning machine and proposed a new hybrid KELM-GA model to deal with the prediction task of BFRC compressive strength. T. Jiang, J.G. Teng et al. [25] improved the algorithm model to provide more accurate prediction of stress-strain behavior for weakly constrained concrete. J. B. Mander et al. [26] proposed a constitutive model of concrete constrained by transverse reinforcement under uniaxial compression, so that the Strain energy in concrete is equal to the Strain energy capacity of transverse reinforcement. XN Bui [27] proposed a new artificial intelligence technology (PSO-KNN) based on Particle Swarm Optimization (PSO) to optimize KNN. We searched and optimized the hyperparameters of KNN using PSO, and obtained different models with three kernel functions: quartic (Q), cubic weighted (T), and cosine (C). By comparing the performance with other machine learning algorithms, the model has been verified to have reliable predictive ability for engineering with explosion safety hazards. HK Kim, Y Lim et al. [28] developed a micro mechanical integrated machine learning method based on experimental evaluation results, which can effectively predict the stress-strain response performance of concrete mixed with crushed clay brick aggregates. Najmoddin Alireza et al. [29] delved into the mechanical characterization of BFRC using six machine learning algorithms (AdaBoost, LightGBM, GBDT, XGBoost, KNN and RF). The novelty lies in the simultaneous prediction of three output variables, compressive, flexural and split tensile strengths, further demonstrating the reliability and simplicity of machine learning. Faruk Ergen et al. [30] investigated the suitability of PSO optimized machine learning models (PSO-RF, PSO-AdaBoost, PSO-XGBoost, PSO-SVR, and PSO-KNN) for predicting shear strength of steel fiber self-compacting concrete (SFR-SCC) beams with/without reinforcement in engineering applications, confirming that the results that the PSO optimization algorithm can be an effective tool to improve the performance of machine learning models. Nima Khodadadi 31 presents an innovative Particle Swarm Classification Boosting Algorithm (PSO-CatBoost) for the prediction of compressive strength of carbon fiber reinforced polymer restrained concrete specimens, which effectively combines the advantages of Particle Swarm Optimization and CatBoost algorithms. The PSO-CatBoost model is then compared with several common algorithmic models, and the results confirm that the optimized model has a higher prediction accuracy, representing a significant shift and development in the research methods available in the field. According to the previous research on machine learning in concrete performance by scholars, machine learning has been commonly used in performance prediction studies of concrete, but there are not many research cases on BFRC using optimization algorithms. The prediction performance of the algorithmic model after optimization algorithm searching and tuning is improved compared to the normal algorithmic model.

The main purpose of this study is to design an accurate and reliable optimization algorithm model to predict the constitutive model of BFRC specimens after compression testing in the MTS816 rock testing system. This has important progressive significance for obtaining experimental data through time-consuming, labor-intensive, and cost-effective experiments. This article obtains experimental data through experiments and establishes an experimental database. Four algorithmic prediction models, PSO-KNN, KNN, support vector regression (SVR), and eXtreme Gradient Boosting (XGB), were established with four main influencing factors on the mechanical behavior of BFRC, namely fiber volume fraction (FVF), fiber length (FL), confining pressure (CP), and strain, as input variables and stress as output variables. After evaluating the model based on performance indicators, select the optimal model to predict the BFRC stress-strain fitting curve. Due to the unique advantages of KNN adapted to this experimental dataset, the prediction effect is better than SVR and XGB, based on which KNN is optimized with PSO to pursue higher prediction accuracy. There is no case study on the stress-strain behavior of BFRC with particle swarm optimization K-nearest neighbor algorithm model, so this study has some novelty and reference significance.

**Table 1**
Main performance indicators of cement.

| Cement varieties | Representation symbol | Specific surface area ($m^2$/kg) | Compressive strength (MPa) | | | Flexural strength (MPa) | | |
|---|---|---|---|---|---|---|---|---|
| | | | 3d | 7d | 28d | 3d | 7d | 28d |
| Composite Portland Cement | P.C42.5 | 36.1 | 23.0 | 34.8 | 46.7 | 5.5 | 6.8 | 9.0 |

**Table 2**
Main performance indicators of basalt fiber.

| Length (mm) | Diameter (μm) | Density (g/$cm^3$) | Operating temperature (°C) | Bonding temperature (°C) | Elastic Modulus (Gpa) | Tensile Strength (Mpa) | Elongation (%) |
|---|---|---|---|---|---|---|---|
| 6/12/18 | 15 | 2.62~2.65 | -269~650 | 1050 | 91~110 | 3000~4800 | 3.14 |

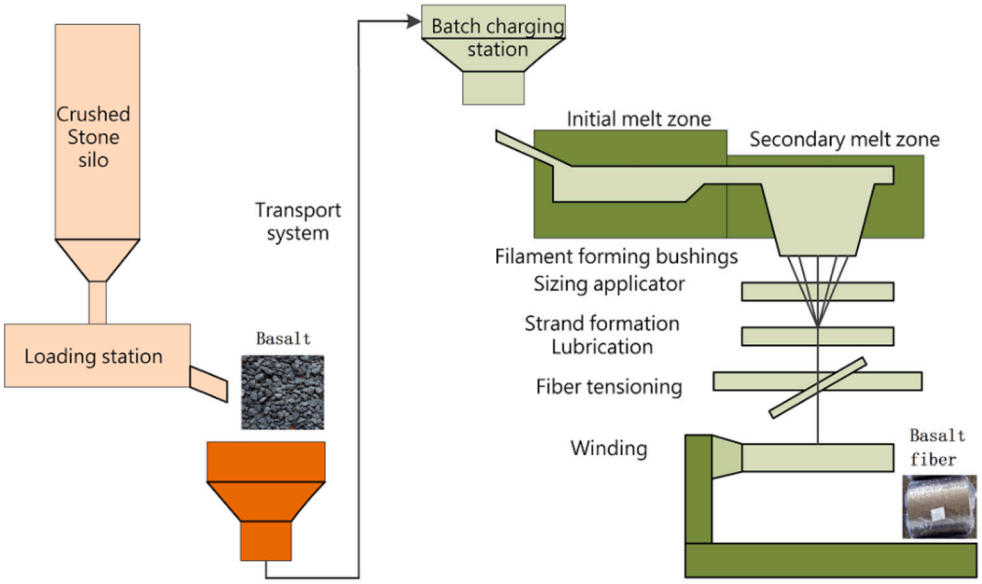


**Fig. 1.** Basalt fiber process flow.

## 2. Data acquisition and analysis

### 2.1. Material parameters and material ratio of the test piece

Cement and BF are the main materials used for specimen preparation, Table 1 and Table 2 correspond to their main performance indicators [1]. Fig. 1 shows the process flow of BF production.

The impact of input parameters on the study of concrete constitutive models is also the main research content of this experiment. Based on scholars' research on the optimal ratio of adding BF to concrete in the past decade [32–39], this article comprehensively selected to conduct uniaxial and conventional triaxial compression tests on BFRC specimens under the conditions of BF volume fraction (0.2%, 0.4%, 0.6%) and BF length (6, 12, 18 mm). The material information used in BFRC is shown in Table 3. Note on specimen number: B represents basalt fiber reinforced concrete; C represents plain concrete, B-6-0.2 represents a doped BF length of 6 mm with a content of 0.2%.

### 2.2. Test process

This study conducted uniaxial and conventional triaxial compression tests on BFRC specimens on MTS816 equipment, with the specific testing process shown in Fig. 2. The BFRC specimens were prepared according to the "Standard for Testing the Performance of Ordinary Concrete Mixtures" (GB50080-2002), and the dimensions of the specimens used in this experiment were all Φ 50×100 (mm). According to the test plan records, tap water, cement, sand, melon seed flakes (coarse aggregate), fly ash, and water reducing agent are mixed with three different lengths of fiber materials, and then a single type of ordinary concrete without BF is mixed separately. After mixing, pour it into a mold to solidify, and take it out for 28 days of specimen curing. Then use a coring machine to cut the concrete sample according to the required size, and then use a grinding machine to polish the end face of the sample until both ends are parallel and smooth. Finally, conduct uniaxial and conventional triaxial compression tests using the MTS816 rock testing system. When conducting uniaxial compression tests, place the concrete specimen at the center of the base; Conducting a triaxial closed test requires applying certain confining pressure to the specimen using closed hydraulic oil pressure, and measuring

**Table 3**
BFRC mix ratio.

| Specimen number | Fiber length (mm) | Fiber content | | Water-cement ratio | cement (kg) | sand (kg) | Coarse aggregate (kg) | Tap water (kg) | Fly ash (kg) | Water reducing agent (kg) |
|---|---|---|---|---|---|---|---|---|---|---|
| | | volume (%) | quality (kg) | | | | | | | |
| C50 | – | - | - | 0.33 | 450 | 682 | 1113 | 150 | 50 | 10.5 |
| B-6-0.2 | | 0.2 | 5.3 | 0.33 | 450 | 682 | 1113 | 150 | 50 | 10.5 |
| B-6-0.4 | 6 | 0.4 | 10.6 | 0.33 | 450 | 682 | 1113 | 150 | 50 | 10.5 |
| B-6-0.6 | | 0.6 | 15.9 | 0.33 | 450 | 682 | 1113 | 150 | 50 | 10.5 |
| B-12-0.2 | | 0.2 | 5.3 | 0.33 | 450 | 682 | 1113 | 150 | 50 | 10.5 |
| B-12-0.4 | 12 | 0.4 | 10.6 | 0.33 | 450 | 682 | 1113 | 150 | 50 | 10.5 |
| B-12-0.6 | | 0.6 | 15.9 | 0.33 | 450 | 682 | 1113 | 150 | 50 | 10.5 |
| B-18-0.2 | | 0.2 | 5.3 | 0.33 | 450 | 682 | 1113 | 150 | 50 | 10.5 |
| B-18-0.4 | 18 | 0.4 | 10.6 | 0.33 | 450 | 682 | 1113 | 150 | 50 | 10.5 |
| B-18-0.6 | | 0.6 | 15.9 | 0.33 | 450 | 682 | 1113 | 150 | 50 | 10.5 |

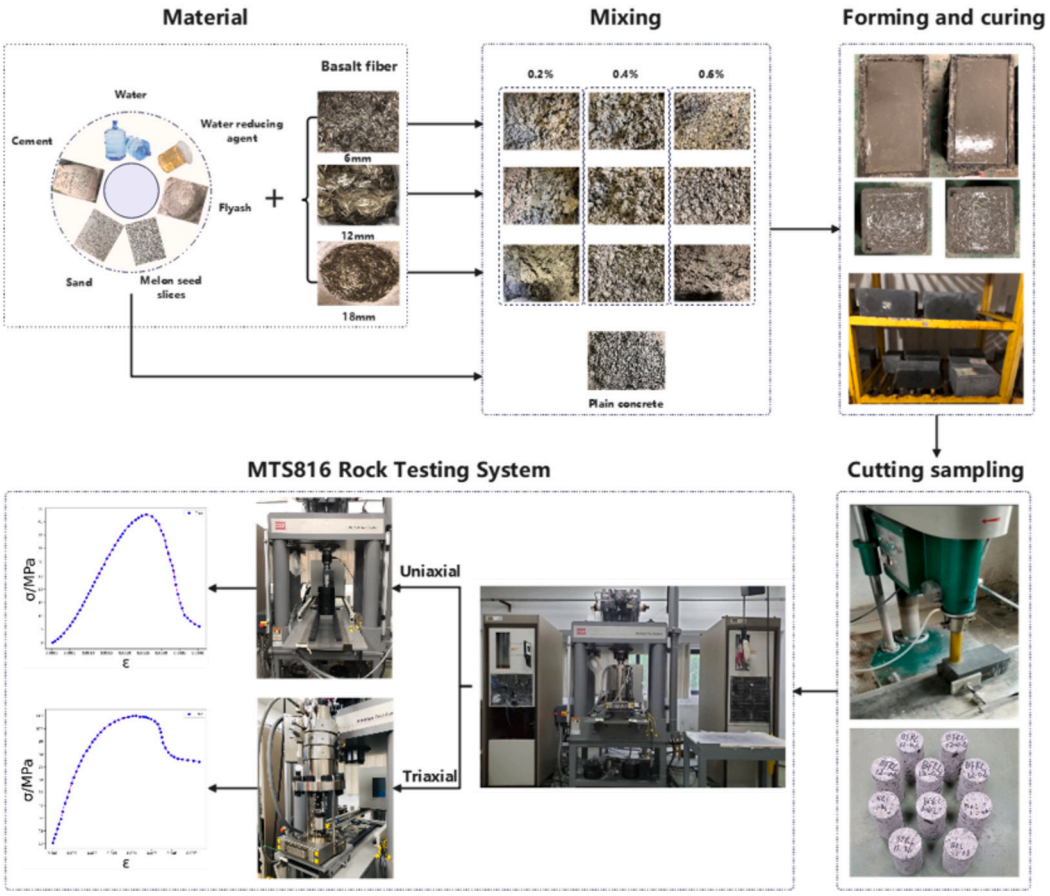


**Fig. 2.** Production and compression process of test pieces.

the deformation of the specimen using circular and radial displacement meters, to obtain the corresponding stress-strain diagram. A total of 1950 sets of data were obtained in this experiment to form the dataset used in the algorithm model of this study.

Fig. 3 shows two typical fiber distribution electron microscope images in basalt fiber concrete, from Fig. 3(a), it can be seen that the basalt fibers are distributed in the form of “bridging” in the cement mortar, basalt fibers are similar to the “bridge” as a connection between the two sides of the cracks in the concrete structure. The basalt fibers connect the concrete structure on both sides of the cracks like a bridge, so that the cracks in the surrounding matrix do not develop further, and the toughness of the concrete structure is enhanced. Fig. 3(b) shows that under the external force, the basalt fibers are presented in the form of fracture, and the basalt fibers do not appear to be pulled out, indicating that the basalt fibers play a certain role in stopping the fracture in the damage process of the specimen.

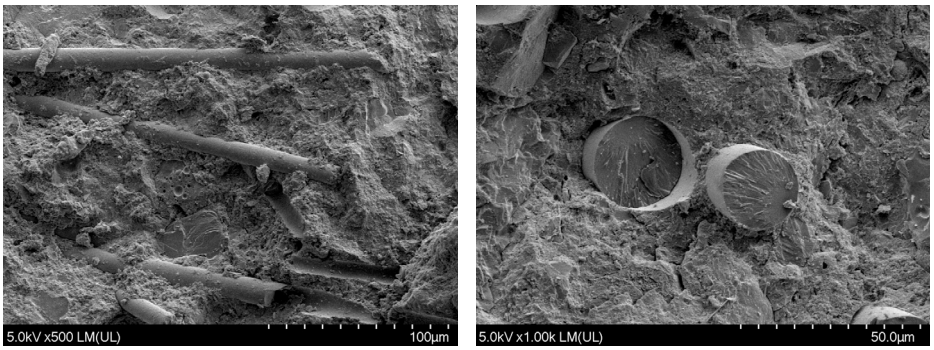


**Fig. 3.** Bridging (a) and fracture (b) morphology of BF inside concrete.

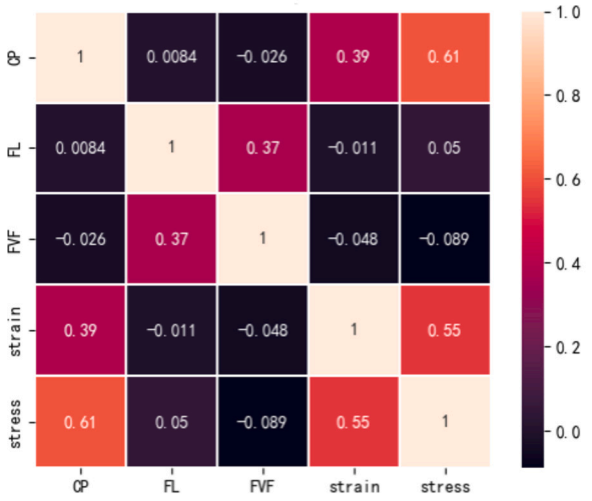


**Fig. 4.** Pearson correlation coefficient.

### 2.3. Correlation analysis

First, divide the 1950 sets of original data set collected by the experiment into 80% training set and 20% test set. To clarify the correlation between the two characteristic parameters, Pearson correlation coefficient [40] is quoted for correlation analysis of four input parameters and the only output parameter. The Pearson correlation coefficient is shown in eq. (1):

$$p = \frac{\sum_{i=1}^{m}(x_i - \bar{x})(y_i - \bar{y})}{\sqrt{\sum_{i=1}^{n}(x_i - \bar{x})^2}\sqrt{\sum_{i=1}^{n}(y_i - \bar{y})^2}} \tag{1}$$

In the formula, M is the number of samples, $y_i$ and $x_i$ are two different eigenvalues, and $\overline{y}$ and $\overline{x}$ are their mean values, respectively.

As shown in Fig. 4, the correlation heat map shows the Pearson coefficient between any two features. It can be seen that among the four input parameters, the correlation between confining pressure and stress is the highest, at 0.61; Next is strain, which is 0.55; The correlation between BF length and BF content and output stress is relatively low.

## 3. Algorithm principles

### 3.1. Extreme gradient enhancement

The extreme gradient lifting principle [41][42] is an Ensemble learning method, which constructs a strong learner by combining multiple weak learners. The core of this algorithm is to improve the model performance step by step through continuous iteration, thereby reaching the limit. In the principle of limit gradient lifting, each weak learner is a decision tree, which is combined to form a strong learner. The formation of all new decision trees is based on the iterative optimization of previous trees. This method can effectively reduce the bias and variance of the model, thereby improving the accuracy of the model.

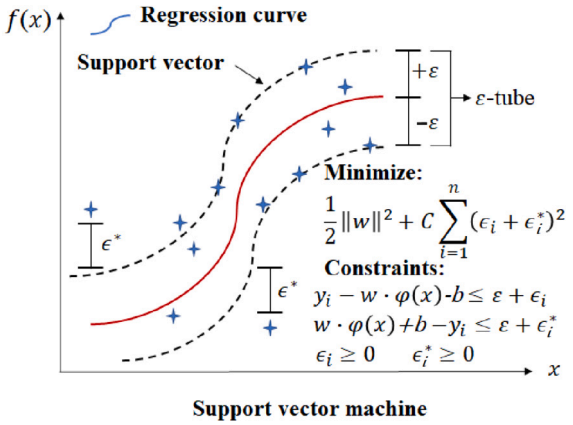


**Fig. 5.** Principle of support vector regression.

XGB also belongs to the Ensemble learning method, and its prediction model and Loss function are similarly applied to the Ensemble learning method. The expression is as follows:

$$\beta_i = \sum_{k=1}^{k} f_k(x_i) \tag{2}$$

$$0\text{bj} = \sum_{i=1}^{n} l(\alpha_i, \beta_i) + \sum_{j=1}^{k} \Omega(f_k) \tag{3}$$

$$\Omega(f_k) = \gamma * T + \frac{1}{2}\lambda \sum_{p=1}^{T} \omega_p^2 \tag{4}$$

In eqs. (2), (3) and (4), K is the number of trees, $f_k$ is the function of the k-th tree, and n is the number of training samples, $\beta_i$ and $\iota(\alpha_i, \beta_i)$ corresponding to the predicted values and training errors of sample $x_i$, where $\Omega(f_k)$ represents the regularization term of $f_k$, i.e. complexity; $\gamma$ and $\lambda$ are parameters that control the severity of punishment, while T and $\omega_p$ are the number and weight of leaf nodes, respectively.

### 3.2. Support vector regression

SVR [43][44] is an important application branch of support vector machine (SVM) models in the field of regression. The concept of SVR is the same as that of SVM. SVR defines the distance from the data point to the boundary of the Hyperplane as the residual. The smaller the residual, the better the regression effect.

As shown in Fig. 5, it is equivalent to taking f(x) as the center, and the two dashed lines are isolation bands with a linear distance of $2\varepsilon$. If the training sample is between the isolation bands, we believe that the prediction is correct, otherwise we calculate the loss. In the equation, C is the regularization constant, $\omega$ and b correspond to weights and biases, $\epsilon$ and $\epsilon_i^*$ is the relaxation variable, $\varphi$(x) is a kernel function. The SVR algorithm is effective in dealing with regression problems of high-dimensional features, but it is sensitive to missing data and can easily cause prediction errors in the model.

### 3.3. K nearest neighbor regression

The K-nearest neighbor method [45] was first proposed by Cover and Hart. KNN not only has simple principle, strong practicability and high precision, but also has no training Time complexity, no data input assumption, and is insensitive to Outlier. KNN can be used for both numerical and discrete data to solve classification and regression tasks. The principle is that a sample should belong to the category that most of its K most similar samples belong to. The distance D between sample points is defined as follows:

$$\mathrm{D}(x_i, y_j) = (\sum_{l=1}^{n} |x_i^l - y_j^l|^p)^{\frac{1}{p}} \tag{5}$$

In Eq. (5), $X_i$ and $y_j$ are any two n-dimensional vectors in the feature space, and p is a distance metric.

The KNN principle flow is shown in Fig. 6.

### 3.4. Particle swarm optimization K nearest neighbor

The particle swarm optimization algorithm [46][47] was first proposed by Kennedy and Eberhar. In this algorithm, each particle only has velocity and position attributes, and continuously updates its attributes through the flow of information within the popu-

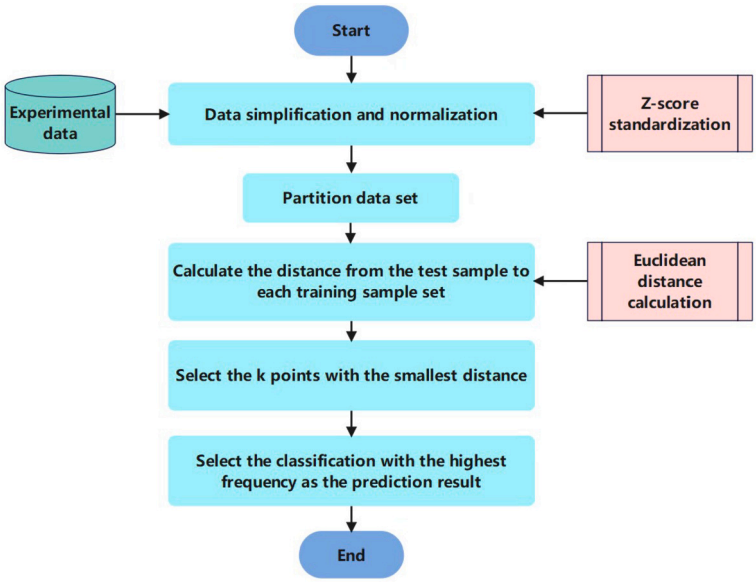


**Fig. 6.** Principle of K-nearest neighbor algorithm.

lation. When one particle in the population determines the global optimal position, other particles will refer to this information to update their two attributes and concentrate on the optimal position. PSO is simple and practical, with fast Rate of convergence and wide application fields. If there are n particles in total and PSO initializes a set of random particles, the position and velocity of the i-th particle in d-dimensional space are represented as follows:

$$V_i^d(t) = \omega V_i^d(t-1) + c_1 r_1 (P_{best}^d - X_i^d(t)) + c_2 r_2 (G_{best}^d - X_i^d(t)) \tag{6}$$

$$X_i^d(t) = X_i^d(t-1) + V_i^d(t) \tag{7}$$

In Eqs. (6) and (7), $V_i^d$(t) and $V_i^d$(t-1) represent the velocities of particles at time t and t-1; $X_i^d$(t) and $X_i^d$(t-1) are the positions of particles at time t and t-1; $P_{best}^d$ and $G_{best}^d$ correspond to local and global optima. $\omega$ represents the inertia coefficient, with a larger value indicating better global search ability and a smaller value indicating better local search ability. $R_1$ and $r_2$ are random numbers between 0 and 1. $C_1$ is an individual learning factor that represents an individual's ability to search for the optimal solution; $C_2$ is a social learning factor that represents the ability of a group to search for optimal solutions. The process of PSO optimization principle is shown in Fig. 7.

After PSO optimization of the KNN model [27], we can determine the optimal hyperparameters of the model. The optimal K value, n_neighbors = 2, select the distance weight as the weight, and the weight is inversely proportional to the sample distance. Under this condition, it is allowed to introduce a distance metric p, p = 2, specified as the Euclidean distance. After dividing the training and testing sets of all models, the random number seed is taken as 42, which can better compare the performance of various models through this parameter selection. The specific process of PSO optimization KNN is shown in Fig. 8.

Fig. 9 shows the flowchart of the four algorithmic models for predicting the BFRC intrinsic model and the direction of the research ideas in this paper.

## 4. Model evaluation

In this study, three model performance indicators, Root mean squared error (RMSE), Mean absolute error (MAE) and Coefficient of determination ($R^2$) [48], were used to evaluate four different algorithms. $R^2$ is widely used in regression homework to evaluate the predictive performance of algorithms and quantify the degree of agreement between actual and predicted values. Both RMSE and MAE are commonly used regression Loss function. The three fitness indicators are all used to evaluate the predictive performance of the model. $R^2$ is between 0 and 1, and the larger the value, the higher the accuracy of the model, while RMSE and MAE are smaller. The expression of these three evaluation indicators is as follows:

$$R^2 = 1 - \frac{\sum_{i=1}^{m} \left(y_i - \hat{y}_i\right)^2}{\sum_{i=1}^{m} (\overline{y} - y_i)^2} \tag{8}$$

$$\mathrm{RMSE} = \sqrt{\frac{1}{m} \sum_{i=1}^{m} \left(y_i - \hat{y}_i\right)^2} \tag{9}$$

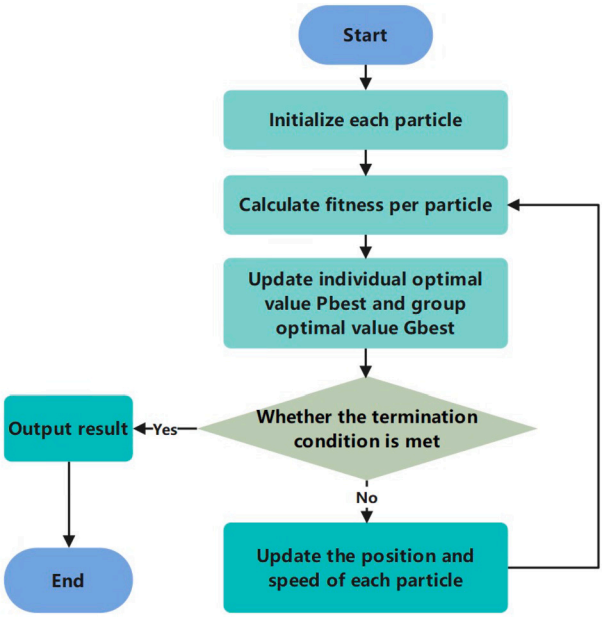


**Fig. 7.** Principle of particle swarm optimization.

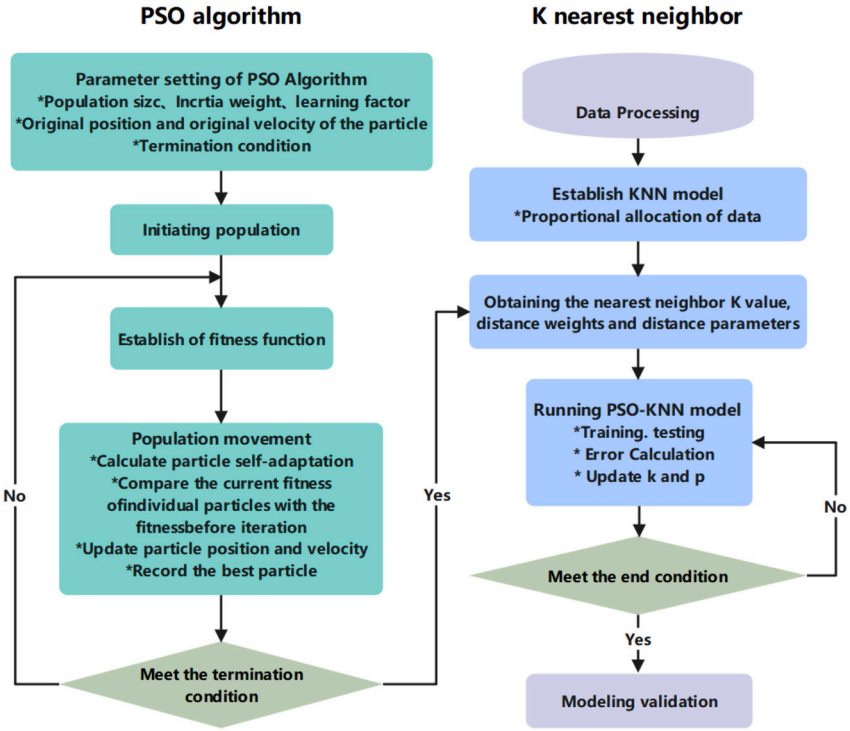


**Fig. 8.** Particle swarm optimization K-nearest neighbor.

$$\mathrm{MAE} = \frac{1}{m}\sum_{i=1}^{m}\left|y_i - \hat{y}_i\right| \tag{10}$$

In Eqs. (8), (9) and (10), m is the number of samples, $y_i$ and $\hat{y}$ are the true and predicted values, respectively, and $\overline{y}$ is the Sample mean.

As shown in Fig. 10(a) to 10(h), the corresponding code edits of the four algorithmic models were used to complete the regression prediction in python software to obtain the regression fitting effects and related data for the training and test sets.

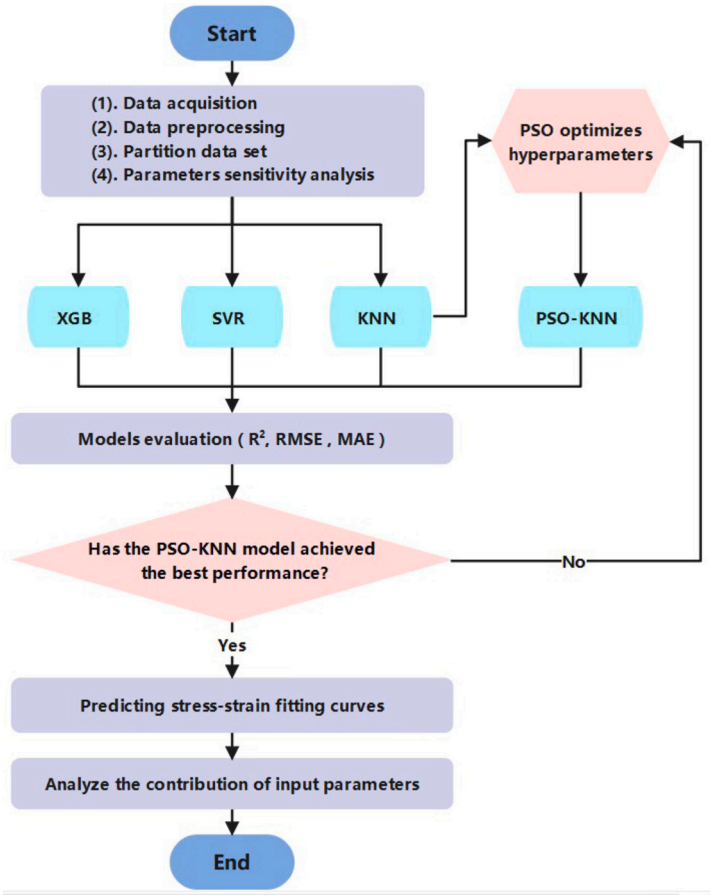


**Fig. 9.** Prediction flow chart of algorithm model.

**Table 4**
Performance parameters of four models.

| | | XGB | SVR | KNN | PSO-KNN |
|---|---|---|---|---|---|
| $R^2$ | train | 0.998 | 0.954 | 0.993 | 1 |
| | test | 0.969 | 0.943 | 0.980 | 0.995 |
| MAE | train | 1.903 | 4.403 | 1.636 | 0.012 |
| | test | 3.966 | 5.121 | 2.902 | 1.138 |
| RMSE | train | 1.567 | 6.833 | 2.703 | 0.182 |
| | test | 5.680 | 7.755 | 4.551 | 2.188 |

Compare the regression prediction results of different models in Fig. 10 on the training and testing sets. It can be seen that in the training set, the fitting accuracy of PSO-KNN and XGB is extremely high, followed by KNN and SVR; The fitting effect of PSO-KNN in the test set is also the best, followed by KNN and XGB. The SVR prediction ability is relatively weak and the fitting is relatively discrete, indicating that the PSO-KNN model has the highest accuracy and performance.

The performance of the comparative model mainly depends on the statistical indicators of the test set. From the radar image of the model in Fig. 11, the size differences of the three corresponding performance indicators for the four models can be compared. Based on the data in Table 4, it can be seen that the RMSE and MAE of the PSO-KNN model on the training set are 0.182 and 0.012, respectively, and the RMSE and MAE on the test set are 2.188 and 1.138, respectively. By comparison, it is evident that the PSO-KNN model has the smallest error values on both the training and testing sets, and the highest score is 0.995, followed by KNN, XGB, and SVR. In terms of performance indicators MAE, PSO-KNN has improved by 60.8%, 71.3%, and 77.8% compared to KNN, XGB, and SVR, respectively, and has improved by 51.9%, 61.5%, and 71.8% in RMSE indicators. Therefore, PSO-KNN has better predictive performance compared to other machine learning algorithms, indicating that this optimized model has good improvement effects and superior application prospects.

In order to observe and compare the predictive performance of these four algorithm models more vividly, while avoiding the blurring and severe overlap of fitting lines caused by excessive data. According to the principle of “rain and dew evenly stained”,

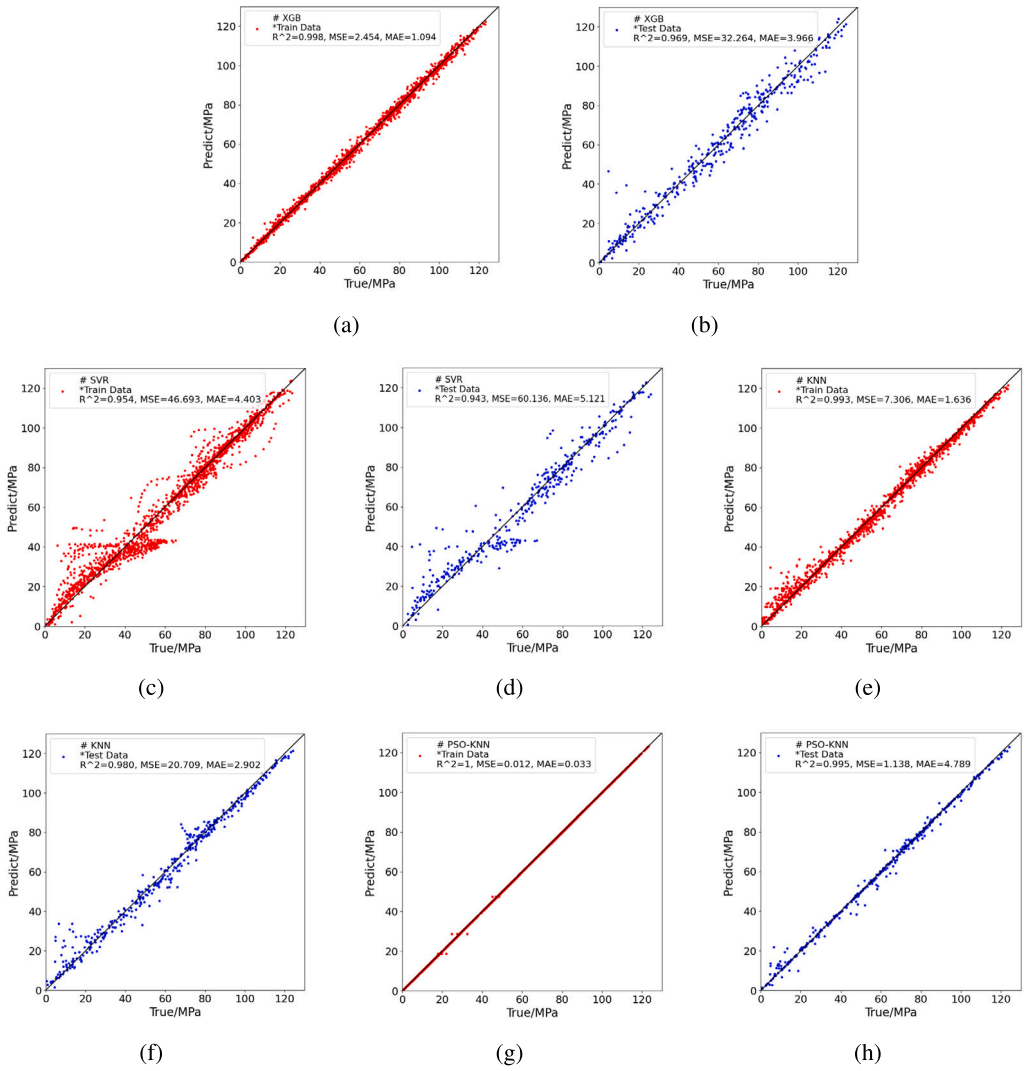


**Fig. 10.** Regression analysis of four models: (a, b) XGB; (c, d) SVR; (e, f) KNN; (g, h) PSO-KNN.

select some data from all data groups for prediction and plotting, and obtain the prediction fitting results in Fig. 12. The prediction performance is determined based on the degree of fitting between the predicted line of four different models and the true value line. It can be seen that the PSO-KNN model has the best fitting effect with the actual line, so its prediction performance is the best. By combining the data from Figs. 9, 10, 11 and Table 4, the strength of the predictive performance of the four algorithm models can be determined: PSO-KNN>KNN>XGB>SVR.

## 5. Predicting the constitutive model of BFRC using PSO-KNN algorithm

### *5.1. PSO-KNN performance analysis*

The previous text has determined that KNN has higher prediction accuracy than XGB and SVR. After PSO optimization, the PSO-KNN model requires better prediction performance. The following residual graph indicates that PSO optimization has achieved smaller prediction errors and better prediction performance.

The comparison of residuals between PSO-KNN and KNN models [49] is shown in Fig. 13. Obviously, the PSO-KNN model has better predictive ability, and the residual fluctuation of the KNN model is relatively large, so PSO optimization has a certain improvement effect.

Fig. 14 shows the prediction results of the PSO-KNN model on the test set data. It can be seen that the predicted values are highly consistent with the actual values, and the overlap effect of the two broken lines is good, which reflects the good predictive performance and high accuracy of the PSO-KNN model. This further indicates the reliability and accuracy of PAO-KNN in predicting the BFRC constitutive model.

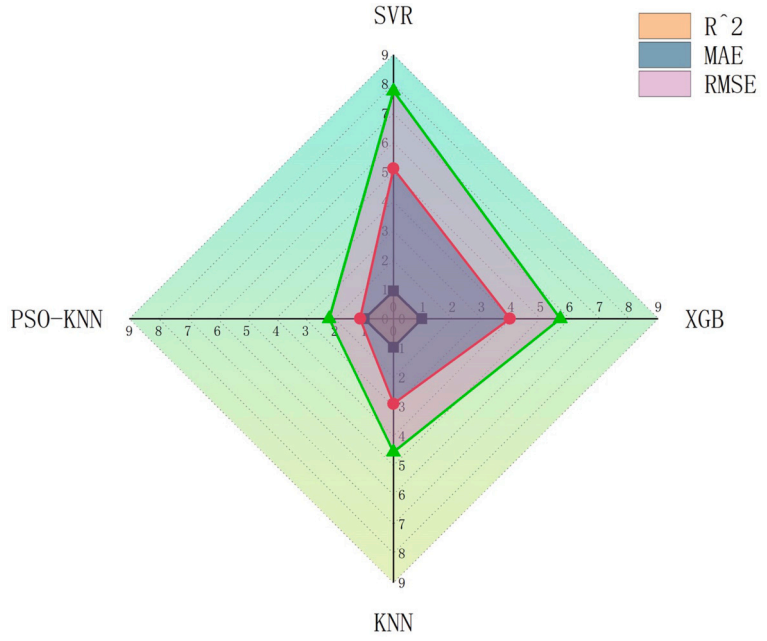


**Fig. 11.** Model radar map.

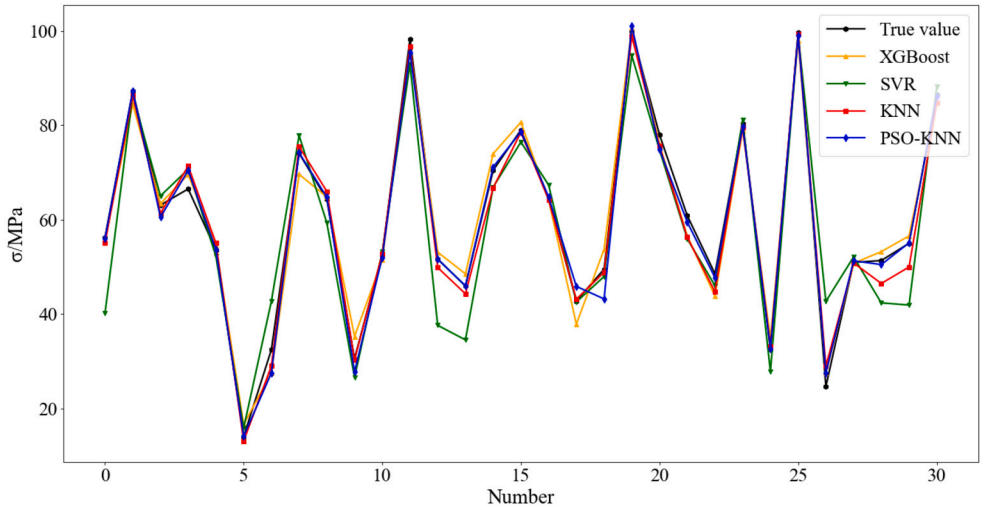


**Fig. 12.** Comparison between models prediction results and actual values.

### *5.2. PSO-KNN predicted stress-strain fitting curve*

This article uses Python software to predict the constitutive model of BFRC. According to the above, the optimal algorithm model PSO-KNN is selected to achieve accurate prediction of the stress-strain fitting curve of BFRC. Note on stress-strain diagram: Example Fig. 15 (e) Title B-5-6-0.6, which means the confining pressure is 5 MPa, the length of BF added is 6 mm, and the proportion of BF is 0.6%.

Each stress-strain curve corresponds to a piece of BFRC specimen, and each curve contains several groups of data, and all the groups of data collected on a piece of specimen are collectively referred to as a specimen group data. Combining the different parameter conditions, the more representative data of 12 specimen groups were selected for graphing, and the predicted results are shown in Figs. 15(a) to 15(l). The curves predicted by the PSO-KNN model fit well with the experimental real curves, and the stress-strain behavior of the BFRC after compression is accurately predicted, and there is basically no difference in the curve trend. Except for a slight difference in the peak strength of the specimen group in Fig. 15(j), the compressive strength predictions for the rest of the specimen groups were accurate.

And based on the principle of control variables, by observing and analyzing the true value curves of all specimen groups, it can be found that the two parameters of circumferential pressure and strain have a more significant effect on stress, i.e., the parameters

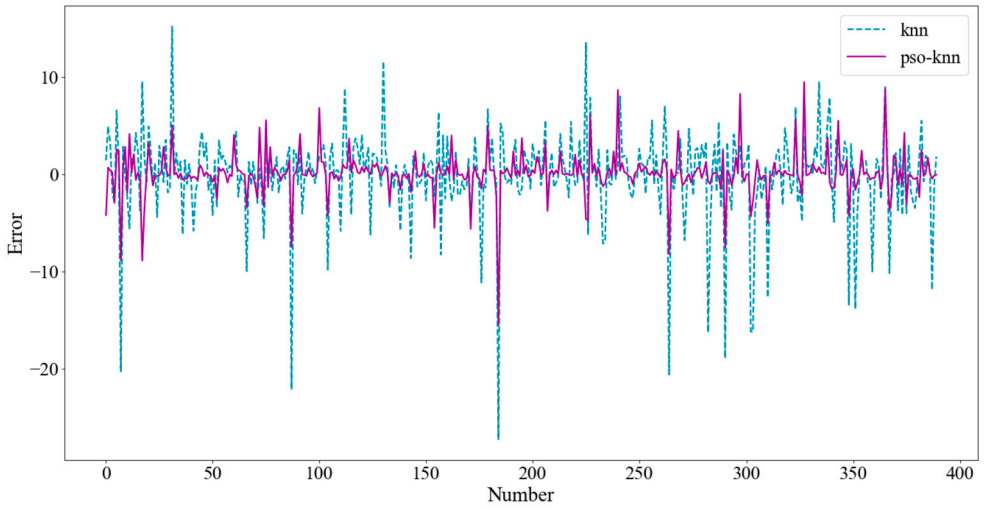


**Fig. 13.** Comparison of residual predictions between KNN and PSO-KNN.

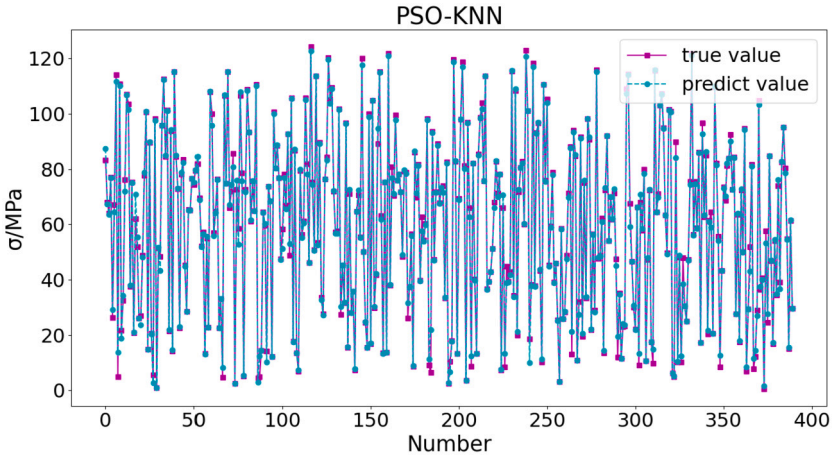


**Fig. 14.** Prediction performance of PSO-KNN model.

are more important, and the parameters of BF content percentage and BF length are less important. It is also confirmed that the optimization algorithm proposed in this paper is able to accurately and reliably predict the macromechanical behavior of BFRC under a variety of test conditions. The algorithm has a strong generalization and promotion ability, which provides a reliable method and basis for the future study of the stress-strain behavior of concrete, and is of great significance for further research expansion by later scholars.

## 6. Conclusion

In this paper, machine learning is introduced on the basis of experiments to establish PSO-KNN, a BFRC mechanical performance prediction model based on particle swarm optimization K-nearest neighbor algorithm. By comparing with KNN, XGB and SVR in terms of RMSE, MAE and $R^2$ performance metrics, it is determined that it has good superiority and thus predicts the intrinsic model of BFRC and the following conclusions are drawn:

(1) Analyzing the magnitude of correlation between input and output parameters by Pearson's coefficient, stress has the highest correlation with perimeter pressure at 0.61, followed by the parameter strain at 0.55, and the input parameter BF length, as well as BF doping, has a lower correlation with stress.

(2) By analyzing the regression prediction performance of the training and testing sets, combined with data analysis of performance indicators $R^2$, MAE, and RMSE, it is known that the PSO-KNN model has the best prediction performance, with $R^2 = 0.995$. According to performance strength, it is ranked as PSO-KNN>KNN>XGB>SVR. In terms of performance indicators MAE, PSO-KNN has improved by 60.8%, 71.3% and 77.8% compared to KNN, XGB, and SVR, respectively. In terms of RMSE indicators, it has improved by 51.9%, 61.5% and 71.8%, indicating a significant improvement in predictive performance.

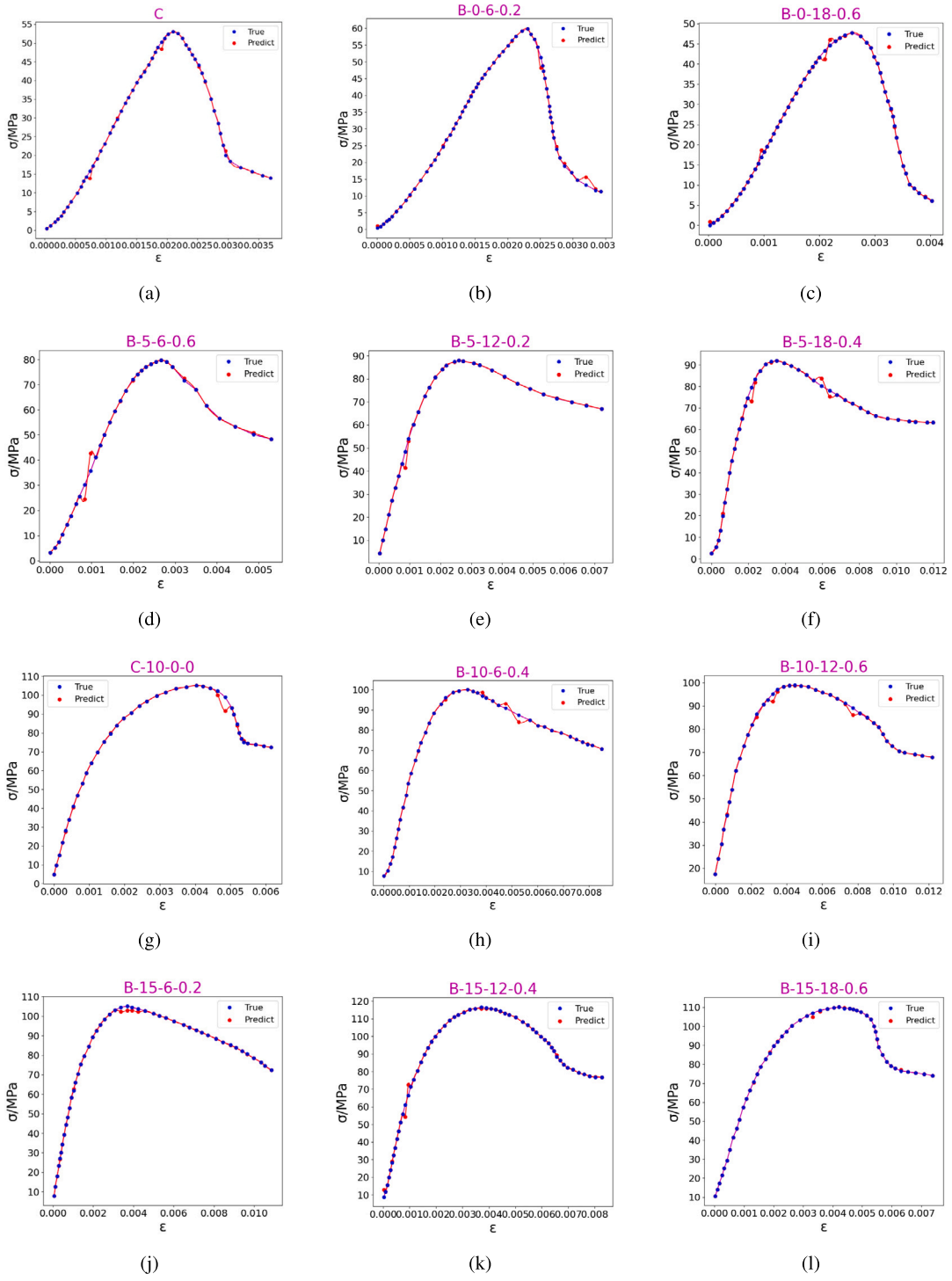


**Fig. 15.** Stress-strain curve of BFRC predicted by PSO-KNN.

(3) The optimized PSO-KNN model has excellent and reliable predictive performance and is more accurate in predicting the stress-strain fitting curve of BFRC after pressure application. By observing and analyzing the true stress-strain curves of all specimen groups, it can be found that the confining pressure and strain parameters have a more significant impact on stress, that is, the importance of the parameters is higher, while the importance of BF content and BF length parameters is lower.

(4) The results of this study confirm that the PSO-KNN model algorithm has a strong generalization and promotion ability, and is highly accurate and reliable in studying the stress-strain behavior of BFRC. The method saves labor, time and expensive cost for

experimental data acquisition, and also provides a basis and reference for subsequent research in this direction and other areas by scholars and engineering applications.

## CRediT authorship contribution statement

**Meng Zhu:** Writing – review & editing, Writing – original draft, Visualization, Validation, Software, Resources, Project administration, Methodology, Investigation, Formal analysis, Data curation, Conceptualization. **Jiajian Lin:** Supervision, Methodology, Investigation, Funding acquisition, Formal analysis, Data curation, Conceptualization. **Guangyong Cao:** Supervision, Methodology, Investigation, Formal analysis, Conceptualization. **Junliang Zhang:** Supervision, Methodology, Formal analysis. **Xin Zhang:** Software, Investigation, Formal analysis. **Jiaxing Zhou:** Supervision, Methodology, Formal analysis, Conceptualization. **Yang Gao:** Supervision, Methodology, Formal analysis, Conceptualization.

## Declaration of competing interest

The authors declare the following financial interests/personal relationships which may be considered as potential competing interests: Lin reports financial support was provided by Anhui University. Jia-jian Lin reports a relationship with Anhui University that includes: funding grants. If there are other authors, they declare that they have no known competing financial interests or personal relationships that could have appeared to influence the work reported in this paper.

## Acknowledgement

This work was supported by the University Synergy Innovation Program of Anhui Province (GXXT-2021-016), the National-Local Joint Engineering Laboratory of Building Health Monitoring and Disaster Prevention Technology (GG19KF001), and the Anhui Province Key Laboratory of Building Structure and Underground Engineering (JD20KF003).

## References

[1] Hong Li, Jiajian Lin, Xiaobao Lei, Tianxia Wei, Compressive strength prediction of basalt fiber reinforced concrete via random forest algorithm, Materials Today Communications 30 (2022) 103117.
[2] Zongwen Li, Jianxun Ma, Hongmin Ma, Xin Xu, Properties and applications of basalt fiber and its composites, IOP Conf. Ser. Earth Environ. Sci. 186 (2018) 012052.
[3] Qiang Liu, Montgomery T. Shaw, Richard S. Parnas, Anne-Marie McDonnell, Investigation of basalt fiber composite mechanical properties for applications in transportation, Polym. Compos. 27 (1) (2006) 41–48.
[4] Tibor Czigány, János Vad, Kornél Pölöskei, Basalt fiber as a reinforcement of polymer composites, Period. Polytech., Mech. Eng. 49 (1) (2005) 3–14.
[5] Dehong Wang, Yanzhong Ju, Hao Shen, Libin Xu, Mechanical properties of high performance concrete reinforced with basalt fiber and polypropylene fiber, Constr. Build. Mater. 197 (2019) 464–473.
[6] Jongsung Sim, Cheolwoo Park, et al., Characteristics of basalt fiber as a strengthening material for concrete structures, Composites, Part B, Eng. 36 (6–7) (2005) 504–512.
[7] Hao Zhou, Bin Jia, Hui Huang, Yanling Mou, Experimental study on basic mechanical properties of basalt fiber reinforced concrete, Materials 13 (6) (2020) 1362.
[8] Sruthi Jalasutram, Dipti Ranjan Sahoo, Vasant Matsagar, Experimental investigation of the mechanical properties of basalt fiber-reinforced concrete, Struct. Concr. 18 (2) (2017) 292–302.
[9] Yan Li, Jiupeng Zhang, Yinzhang He, Guojing Huang, Junbo Li, Zhenxing Niu, Bo Gao, A review on durability of basalt fiber reinforced concrete, Compos. Sci. Technol. (2022) 109519.
[10] Yong Xin Yang, Jie Lian, Basalt fiber reinforced concrete, in: Advanced Materials Research, vol. 194, Trans. Tech. Publ., 2011, pp. 1103–1108.
[11] Chunmei Gao, Weijie Wu, Using esem to analyze the microscopic property of basalt fiber reinforced asphalt concrete, International Journal of Pavement Research and Technology 11 (4) (2018) 374–380.
[12] Wenjing Wang, Lin Zhao, Yuanzhen Liu, Zhu Li, Mechanical properties and stress–strain relationship in axial compression for concrete with added glazed hollow beads and construction waste, Constr. Build. Mater. 71 (2014) 425–434.
[13] Sandor Popovics, A review of stress-strain relationships for concrete, Journal Proceedings 67 (1970) 243–248.
[14] Sandor Popovics, A numerical approach to the complete stress-strain curve of concrete, Cem. Concr. Res. 3 (5) (1973) 583–599.
[15] Seong-Tae Yi, Jin-Keun Kim, Tae-Keun Oh, Effect of strength and age on the stress–strain curves of concrete specimens, Cem. Concr. Res. 33 (8) (2003) 1235–1244.
[16] Guo Zhenhai Zhang, Xiuqin Zhang Dacheng, Wang Ruqi, Experimental investigation of the complete stress-strain curve of concrete, J. Build. Struct. 3 (01) (1982) 1.
[17] Chaohua Jiang, Ke Fan, Fei Wu, Da Chen, Experimental study on the mechanical properties and microstructure of chopped basalt fibre reinforced concrete, Mater. Des. 58 (2014) 187–193.
[18] Zühtü Onur Pehlivanlı, Ibrahim Uzun, Ilhami Demir, Mechanical and microstructural features of autoclaved aerated concrete reinforced with autoclaved polypropylene, carbon, basalt and glass fiber, Constr. Build. Mater. 96 (2015) 428–433.
[19] Ahmet B. Kizilkanat, Nihat Kabay, Veysel Akyüncü, Swaptik Chowdhury, Abdullah H. Akça, Mechanical properties and fracture behavior of basalt and glass fiber reinforced concrete: an experimental study, Constr. Build. Mater. 100 (2015) 218–224.
[20] Shaozheng Yu, Yingqiu Li, Guojun Sheng, Jiao Lv, Research on short-term traffic flow forecasting based on knn and discrete event simulation, in: Advanced Data Mining and Applications: 15th International Conference, ADMA 2019, Dalian, China, in: Proceedings 15, November 2019, pp. 21–23, Springer, 2019, pp. 853–862.
[21] John Östh, William AV Clark, Bo Malmberg, Measuring the scale of segregation using k-nearest neighbor aggregates, Geogr. Anal. 47 (1) (2015) 34–49.
[22] Rod E. Turochy, Benjamin D. Pierce, Relating short-term traffic forecasting to current system state using nonparametric regression, in: Proceedings. The 7th International IEEE Conference on Intelligent Transportation Systems (IEEE Cat. No. 04TH8749), IEEE, 2004, pp. 239–244.
[23] I. Kinder, Kresimir Friganovic, J. Vukojevic, D. Mulc, T. Slukan, D. Vidovic, P. Brecic, Mario Cifrek, Comparison of machine learning methods in classification of affective disorders, in: 2020 43rd International Convention on Information, Communication and Electronic Technology (MIPRO), IEEE, 2020, pp. 177–181.

[24] Hong Li, Jiajian Lin, Dawei Zhao, Guodong Shi, Haibo Wu, Tianxia Wei, Dailin Li, Junliang Zhang, A bfrc compressive strength prediction method via kernel extreme learning machine-genetic algorithm, Constr. Build. Mater. 344 (2022) 128076.
[25] T. Jiang, J.G. Teng, Analysis-oriented stress–strain models for frp–confined concrete, Eng. Struct. 29 (11) (2007) 2968–2986.
[26] John B. Mander, Michael J.N. Priestley, R. Park, Theoretical stress-strain model for confined concrete, J. Struct. Eng. 114 (8) (1988) 1804–1826.
[27] Xuan-Nam Bui, Pirat Jaroonpattanapong, Hoang Nguyen, Quang-Hieu Tran, Nguyen Quoc Long, A novel hybrid model for predicting blast-induced ground vibration based on k-nearest neighbors and particle swarm optimization, Sci. Rep. 9 (1) (2019) 1–14.
[28] Hyeong-Ki Kim, Yeonggyu Lim, Million Tafesse, G.M. Kim, Beomjoo Yang, Micromechanics-integrated machine learning approaches to predict the mechanical behaviors of concrete containing crushed clay brick aggregates, Constr. Build. Mater. 317 (2022) 125840.
[29] Alireza Najmoddin, Hossein Etemadfard, Mansour Ghalehnovi, et al., Multi-output machine learning for predicting the mechanical properties of bfrc, Case Studies in Construction Materials 20 (2024) e02818.
[30] Faruk Ergen, Metin Katlav, Investigation of optimized machine learning models with pso for forecasting the shear capacity of steel fiber-reinforced scc beams with/out stirrups, J. Build. Eng. 83 (2024) 108455.
[31] Nima Khodadadi, Hossein Roghani, Francisco De Caso, El-Sayed M. El-kenawy, Yelena Yesha, Antonio Nanni, Data-driven pso-catboost machine learning model to predict the compressive strength of cfrp-confined circular concrete specimens, Thin-Walled Struct. (2024) 111763.
[32] Mahzabin Afroz, Indubhushan Patnaikuni, Srikanth Venkatesan, Chemical durability and performance of modified basalt fiber in concrete medium, Constr. Build. Mater. 154 (2017) 191–203.
[33] Xinzhong Wang, Jun He, Ayman S. Mosallam, Chuanxi Li, Haohui Xin, The effects of fiber length and volume on material properties and crack resistance of basalt fiber reinforced concrete (bfrc), Adv. Mater. Sci. Eng. 2019 (2019) 1–17.
[34] Ahmed M. Tahwia, Khaled A. Helal, Osama Youssf, Chopped basalt fiber-reinforced high-performance concrete: an experimental and analytical study, Journal of Composites Science 7 (6) (2023) 250.
[35] Wei Chen, Zi Chong Zhu, Jun Wang, Jia Chen, You Mo, Numerical analysis of mechanical properties of chopped basalt fiber reinforced concrete, in: Key Engineering Materials, vol. 815, Trans. Tech. Publ., 2019, pp. 175–181.
[36] Lei Gao, Guohui Hu, Nan Xu, Junyi Fu, Chao Xiang, Chen Yang, Experimental study on unconfined compressive strength of basalt fiber reinforced clay soil, Adv. Mater. Sci. Eng. (2015, 2015).
[37] Jian-jun Li, Zhi-ming Zhao, Study on mechanical properties of basalt fiber reinforced concrete, in: 2016 5th International Conference on Environment, Materials, Chemistry and Power Electronics, Atlantis Press, 2016, pp. 406–410.
[38] Xinjian Sun, Zhen Gao, Peng Cao, Changjun Zhou, Mechanical properties tests and multiscale numerical simulations for basalt fiber reinforced concrete, Constr. Build. Mater. 202 (2019) 58–72.
[39] Muhammad Riaz Ahmad, Bing Chen, Effect of silica fume and basalt fiber on the mechanical properties and microstructure of magnesium phosphate cement (mpc) mortar, Constr. Build. Mater. 190 (2018) 466–478.
[40] David Corr, Matteo Accardi, Lori Graham-Brady, Surendra Shah, Digital image correlation analysis of interfacial debonding properties and fracture behavior in concrete, Eng. Fract. Mech. 74 (1–2) (2007) 109–121.
[41] Wei Dong, Yimiao Huang, Barry Lehane, Guowei Ma, Xgboost algorithm-based prediction of concrete electrical resistivity for structural health monitoring, Autom. Constr. 114 (2020) 103155.
[42] Jin Duan, Panagiotis G. Asteris, Hoang Nguyen, Xuan-Nam Bui, Hossein Moayedi, A novel artificial intelligence technique to predict compressive strength of recycled aggregate concrete using ica-xgboost model, Eng. Comput. 37 (2021) 3329–3346.
[43] Prasenjit Saha, Prasenjit Debnath, Paul Thomas, Prediction of fresh and hardened properties of self-compacting concrete using support vector regression approach, Neural Comput. Appl. 32 (12) (2020) 7995–8010.
[44] Hemn Unis Ahmed, Reham R. Mostafa, Ahmed Mohammed, Parveen Sihag, Azad Qadir, Support vector regression (svr) and grey wolf optimization (gwo) to predict the compressive strength of ggbfs-based geopolymer concrete, Neural Comput. Appl. 35 (3) (2023) 2909–2926.
[45] Kenneth Jae T. Elevado, Joenel G. Galupino, Ronaldo S. Gallardo, Compressive strength modelling of concrete mixed with fly ash and waste ceramics using k-nearest neighbor algorithm, GEOMATE Journal 15 (48) (2018) 169–174.
[46] Qinghai Bai, Analysis of particle swarm optimization algorithm, Comput. Inf. Sci. 3 (1) (2010) 180.
[47] Wan-Li Zuo, Zhi-Yan Wang, Tong Liu, Hui-Ling Chen, Effective detection of Parkinson's disease using an adaptive fuzzy k-nearest neighbor approach, Biomed. Signal Process. Control 8 (4) (2013) 364–373.
[48] Jozsef Pap, Csaba Mako, Miklos Illessy, Norbert Kis, Amir Mosavi, Modeling organizational performance with machine learning, Journal of Open Innovation: Technology, Market, and Complexity 8 (4) (2022) 177.
[49] Odey Alshboul, Ali Shehadeh, Maha Al-Kasasbeh, Rabia Emhamed Al Mamlook, Neda Halalsheh, Muna Alkasasbeh, Deep and machine learning approaches for forecasting the residual value of heavy construction equipment: a management decision support model, Eng. Constr. Archit. Manag. 29 (10) (2022) 4153–4176.